

Human Balancing on a Log: A Switched Multi-Layer Controller

Jiayi Zhao, Mo Yang, Jing Shuang (Lisa) Li

Abstract—We study the task of balancing a human on a log that is fixed in place. Balancing on a log is substantially more challenging than balancing on a flat surface — to achieve stability, we use a switched multi-layer controller. The controller consists of an upper-layer LQR planner (akin to the central nervous system) that coordinates ankle and hip torques, and lower-layer PID trackers (akin to local motor units) that follow this plan subject to nonlinear dynamics. Additionally, the controller switches between three operational modes depending on the current state of the human. The efficacy of the controller is verified in simulation, where our controller is able to stabilize the human for a variety of initial conditions. We also show that this controller is compatible with muscle-based actuation and imperfect sensing, making it a promising candidate for modeling motor control under challenging conditions in a more bio-realistic way.

I. INTRODUCTION

Postural balancing is an important part of everyday life — most humans stand and balance with ease. This task is extensively studied, with the goal of improving our scientific understanding of motor control, and to gain insights which may be applicable to robotic balancing [1]–[6]. Typically, models of postural balancing involve balancing on flat ground [3]–[6]. Most models make simplifying assumptions that result in an inverted pendulum model [3], [5], [6], while other models incorporate more biomechanical details [4]. Optimal control strategies are frequently used [5], [6], as well as switched strategies [2].

We are interested in the problem of balancing on a log that is fixed in place, as shown in Figure 1. While this task is significantly more difficult than balancing on flat ground, most individuals with sufficient fitness and coordination can maintain balance for at least several seconds — thus, we want to provide a control strategy that replicates human ability to balance in this scenario. The difficulty of this task is embodied by its highly unstable dynamics, in which even small deviations from equilibrium result in rapidly growing accelerations. Here, manipulating ankle torque alone is insufficient for stability; we also require torque from the hip joint.

Our controller is inspired by animal sensorimotor control, which features multiple layers. Upper layers (e.g. central nervous system) are responsible for planning and coordination across body parts, while lower layers (e.g. motor units associated with individual joints and muscles) are responsible for carrying out these plans for individual body parts [7], [8]. In our controller, we use an upper-layer linear quadratic regulator (LQR) and lower-layer proportional-integral-derivative

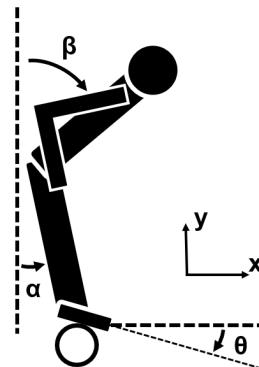


Fig. 1. Schematic of a human balancing on a log. The log is fixed in place and does not roll. θ indicates angular deviation of the foot from the x axis, and α and β indicate angular deviations from the y axis for the leg and torso, respectively. We use a right-hand sign convention for angles; in this image, β and θ have negative values.

(PID) controller (described in Section III). In addition to being multi-layered, our controller also switches between different operational modes depending on the current state of the human, leveraging ideas from switched strategies in postural control [2]. We demonstrate that our controller is able to stabilize the system for a variety of initial conditions in Section IV, and describe how the controller can be made more biologically plausible (e.g. incorporate muscle-based actuation and imperfect sensing) in Section V.

II. PROBLEM SETUP

We consider a human balancing on a log that is fixed in place and does not roll, as depicted in Figure 1. We confine ourselves to analysis in the depicted 2-D plane, and assume that the foot does not slip on the log. In this model, the body contains three mass points, located at the head, hip and ankle. The knees are assumed to be straight, and there is no hand or arm motion; the hip and ankle are free to rotate.

The angles of interest are θ , α , and β . θ indicates angular deviation of the foot from the x axis, and α and β indicate angular deviations from the y axis for the leg and torso, respectively. Note that these are global angles; they can be easily converted to and from body angles. Specifically, hip angle can be expressed as $\pi - \alpha + \beta$, and ankle angle can be expressed as $0.5\pi + \alpha - \theta$. In our analysis, the equilibrium posture of the human consists of a foot that is parallel with the ground, a leg vertical to the ground, and a torso that is slightly leaning forward, as shown in the top of 3.

Our controller makes use of both angles and center of mass (COM) measurements. We use COM_x to refer to the

*All authors are with the Department of Electrical Engineering and Computer Science at the University of Michigan. zjiay@umich.edu, sprkyang@umich.edu, jslisali@umich.edu

projection of the center of mass on the x axis, and similarly for COM_y ; the controller is concerned only with COM_x , which determines the stability of the human. The controller applies two torques: the ankle torque τ_1 and hip torque τ_2 . The goal of the controller is to restore the human to the equilibrium posture, subject to the equations of motion:

$$\begin{aligned}
x_0 &= -r \sin \theta + \theta r \cos \theta - l_0 \cos \theta \\
y_0 &= r \cos \theta + \theta r \sin \theta - l_0 \sin \theta \\
x_1 &= x_0 - l_1 \sin \alpha \\
y_1 &= y_0 + l_1 \cos \alpha \\
x_2 &= x_1 - l_2 \sin \beta \\
y_2 &= y_1 + l_2 \cos \beta \\
\tau_1 &= -\ddot{x}_2 m_2 (l_2 \cos \beta + l_1 \cos \alpha) \\
&\quad - m_2 (\ddot{y}_2 + g) (l_2 \sin \beta + l_1 \sin \alpha) \\
&\quad - \ddot{x}_1 l_1 m_1 \cos \alpha - (\ddot{y}_1 + g) l_1 m_1 \sin \alpha \\
\tau_2 &= -\ddot{x}_2 l_2 m_2 \cos \beta - (\ddot{y}_2 + g) l_2 m_2 \sin \beta \\
\text{COM}_x &= \frac{x_0 m_0 + x_1 m_1 + x_2 m_2}{m_0 + m_1 + m_2} \\
\text{COM}_y &= \frac{y_0 m_0 + y_1 m_1 + y_2 m_2}{m_0 + m_1 + m_2} \\
N_x &= \frac{\tau_1}{r \theta - l_0} \sin \theta \\
N_y &= \frac{\tau_1}{l_0 - r \theta} \cos \theta \\
f_x + N_x &= \ddot{x}_0 m_0 + \ddot{x}_1 m_1 + \ddot{x}_2 m_2 \\
f_y + N_y &= (\ddot{y}_0 + g) m_0 + (\ddot{y}_1 + g) m_1 + (\ddot{y}_2 + g) m_2 \\
f_y &= f_x \tan \theta \\
N_x^2 + N_y^2 &= N_x (\ddot{x}_0 m_0 + \ddot{x}_1 m_1 + \ddot{x}_2 m_2) \\
&\quad + N_y [(\ddot{y}_0 + g) m_0 + (\ddot{y}_1 + g) m_1 + (\ddot{y}_2 + g) m_2] \\
0 &= (f_y + N_y) (\text{COM}_x - r \sin \theta) \\
&\quad + (f_x + N_x) (\text{COM}_y - r \cos \theta) \\
&\quad - \ddot{x}_0 m_0 (\text{COM}_y - y_0) \\
&\quad - \ddot{x}_1 m_1 (\text{COM}_y - y_1) \\
&\quad - \ddot{x}_2 m_2 (\text{COM}_y - y_2) \\
&\quad - \ddot{y}_0 m_0 (x_0 - \text{COM}_x) \\
&\quad - \ddot{y}_1 m_1 (x_1 - \text{COM}_x) \\
&\quad - \ddot{y}_2 m_2 (x_2 - \text{COM}_x)
\end{aligned} \tag{1}$$

where x_i and y_i are the projections of the i^{th} mass point on the x and y axes respectively, m_i are the masses of the mass points. l_i are the distances from the i^{th} mass to the $(i-1)^{\text{th}}$ mass; l_0 is the distance of the 1st mass point to the point of contact. r is the radius of the log. τ_1 and τ_2 are the torques on the two joints. f_x and f_y are friction forces along the x and y axes respectively; similarly, N_x and N_y are the normal forces from the log to the foot projected along the relevant axes.

III. METHODOLOGY

Inspired by multi-layer processing in animal sensorimotor control, we propose a two-layer controller, shown in Figure

2. The controller's inputs are the COM, angle, and angular velocity states (i.e. $\text{COM}_x, \theta, \alpha, \beta, \dot{\theta}, \dot{\alpha}, \dot{\beta}$); the controller outputs torques on the two joints (i.e. τ_1, τ_2). Our controller consists of a central planner, which uses COM information to compute target angle(s), and local trackers, which track these angles for the joints. The local trackers do not coordinate with one another. While the central planners operate on linear approximations, the local trackers operate on the true nonlinear system described by (1). Overall, the central planners use linear approximations and LQR to facilitate smooth convergence of the COM value to equilibrium, while the local trackers use PID control handle the nonlinearities inherent in the system, particularly at large COM values; the combined controller performs better than LQR or PID alone.

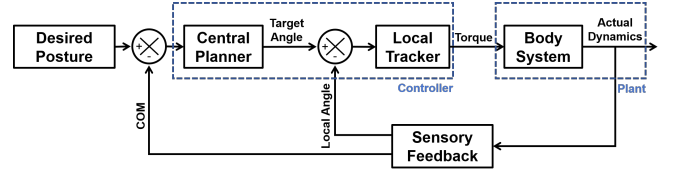


Fig. 2. General two-layer control strategy. The upper layer ('Central Planner') produces target angles; errors between target angles and actual angles are sent to the lower layer ('Local Tracker'), which directly acts on the body to track the target angles. The overall controller receives both COM information and angle information from the body via sensory feedback.

We apply a switched controller to this system. This controller can stabilize the system to a pre-defined equilibrium from any initial position within a certain range, and can tolerate disturbance and noise — this is shown in Section IV. There are 3 cases in the switched controller:

- Case 1: The body COM and torso angle are close to equilibrium; the Case 1 controller keeps the states near equilibrium. Generally, if disturbances are infrequent, the Case 1 controller is used most of the time. In the absence of disturbances, the Case 1 controller keeps the switched controller in Case 1 for all time.
- Case 2. The body COM is far from equilibrium. In this case, the person is in immediate danger of falling over; the Case 2 controller aims to quickly reduce COM deviation from equilibrium. Generally, the Case 2 controller is used immediately after a large initial condition or perturbation.
- Case 3. The body COM is close to equilibrium, but the torso angle is far from equilibrium. In this case, the person is not in immediate danger of falling over, but is also not in the ideal state. The Case 3 controller restores the torso angle to equilibrium while keeping the COM close to equilibrium. The Case 3 controller is used immediately after Case 2.

A switching controller is required because a single offline controller cannot effectively handle all 3 cases, which have different objectives and varying requirements on response time. For instance, Case 2 requires a fast, aggressive action, while Case 3 requires slower coordination between hip and ankle to ensure that while restoring the torso angle, we do not

Case	Condition	Hip Controls	Ankle Controls
1	$ \text{COM}_x \leq 0.04m$, $ \beta - \beta_0 < 0.1$	Planner: N/A, Tracker: Stiff	Planner: LQR, Tracker: PID
2	$ \text{COM}_x > 0.04m$, $ \beta - \beta_0 < 1.0$	Planner: LQR, Tracker: N/A	Planner: Linear, Tracker: PID
3	$ \text{COM}_x \leq 0.04m$, $ \beta - \beta_0 > 0.005$	Planner: LQR, Tracker: N/A	Planner: LQR, Tracker: PID

TABLE I

SWITCHED 3-CASE CONTROLLER: CONDITIONS AND CORRESPONDING ACTIONS.

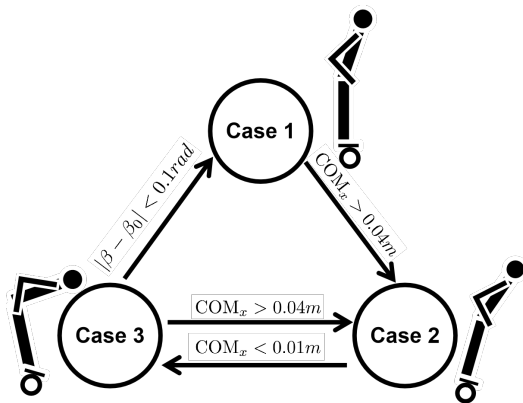


Fig. 3. Transition rules between the three cases of the switched controller. Each case is accompanied by a depiction of the human’s posture in that case.

cause COM deviations. In contrast, Case 1 (which is the case generally studied in literature) does not require substantial coordination between these entities.

The three cases and their associated controllers are shown in Table I, and the switching rules are shown in Figure 3. We note that there is no direct transition from Case 2 to Case 1. This is because the Case 2 controller leverages hip movement to aggressively control COM — this never results in a torso angle that is close to equilibrium (as Case 1 requires). There is also no direct transition from Case 1 to Case 3 — such a transition is improbable, as it is unlikely that a disturbance would affect torso angle but not COM. In general, for some impulsive disturbance, the controller starts with Case 2, then transitions to Case 3, then to Case 1. Once in Case 1, it stays in Case 1 until another disturbance is encountered. We also observed in simulations that a transition from Case 3 to 2 is relatively rare.

We now detail the controllers used for each case.

A. Case 1

The Case 1 controller is applied when both COM and torso angle are close to equilibrium. This controller keeps these values close to equilibrium. We use a controller that primarily uses ankle torque; we apply a hip torque controller that makes the hip angle $\theta_2 = \beta - \alpha$ stiff, as follows:

$$\tau_2 = -k_p \theta_2 - k_d \dot{\theta}_2 \quad (2)$$

For large k_p and k_d , the hip is stiff. This allows us to model body dynamics as an inverted single pendulum, as

is commonly done in the literature on balancing.

We use an LQR controller in the upper layer. To apply LQR, we build a linear model of state dynamics; the states are COM_x . Consider the inverted single pendulum with rod length L , where the pivot x_{contact} is free to move along the x -axis. We will treat x_{contact} as the input for the LQR model. Let x be the mass point’s projection onto the x -axis. The equation of motion for the COM is:

$$\frac{d^2 \text{COM}_x}{dt^2} = g(\text{COM}_x - x_{\text{contact}})/L \quad (3)$$

This is a linear equation of motion; we apply LQR to obtain a controller. We use state penalties on the order of 100 times the input penalty.

Now, consider a person standing on a log. In this case, the projection of the pivot point onto the x -axis can be expressed as $x_{\text{contact}} = -r \sin \theta$, where r is the radius of the log. To retrieve the desired angle θ from the LQR output, we use

$$\theta = \sin^{-1}(x_{\text{contact}}/r) \quad (4)$$

This desired angle is then tracked by the PID controller. The dynamics of the foot angle are complicated — in lieu of analyzing and attempting to linearize these dynamics, we directly tuned a PID controller in simulation to track the desired foot angle by outputting the appropriate ankle torque τ_1 . We note that the foot angle dynamics have relatively small influence on the upper body — thus, its influence can be ignored by the upper-level LQR planner.

Remark: Case 1 can also be handled without considering COM directly (see Section V); in general, there are several ways to stabilize for Case 1. Here, the mathematical setup for Case 1 will be re-used in Case 3, where COM is very much required.

B. Case 2

The Case 2 controller is applied when the COM is far from equilibrium. This controller aims to quickly reduce the COM deviation from equilibrium to prevent the person from falling.

Similar to Case 1, we can use an LQR controller for the upper layer. The states are COM_x and its derivative. In this case, the equations of motion simplify to

$$\frac{d^2 \text{COM}_x}{dt^2} = C_1 \tau_2 \quad (5)$$

where C_1 is some constant. We now show this.

We make simplifying assumptions on (1) to produce the equations of motion for a double pendulum. Since this controller acts very quickly, we ignore the influence of

gravity (and therefore, of θ).

$$\begin{aligned}
F_x &= \ddot{x}_2 m_2 + \ddot{x}_1 m_1 \\
F_y &= \ddot{y}_2 m_2 + \ddot{y}_1 m_1 \\
-\frac{\tau_2}{l_2} &= \ddot{x}_2 m_2 \cos \beta + \ddot{y}_2 \sin \beta \\
\ddot{\beta} l_2^2 \frac{m_1 m_2}{m_1 + m_2} &= F_x (l_1 \cos \alpha + l_2 \frac{m_2}{m_1 + m_2} \cos \beta) \\
&\quad + F_y (l_1 \sin \alpha + l_2 \frac{m_2}{m_1 + m_2} \sin \beta) \\
\text{COM}_x &= \frac{x_1 m_1 + x_2 m_2}{m_0 + m_1 + m_2}
\end{aligned} \tag{6}$$

For α and β both small, we have

$$\begin{aligned}
\ddot{\beta} l_2^2 \frac{m_1 m_2}{m_1 + m_2} &= F_x (l_1 + l_2 \frac{m_2}{m_1 + m_2}) \\
F_x &= -\ddot{\alpha} l_1 m_2 - \ddot{\beta} l_2 m_2 - \ddot{\alpha} l_1 m_1 \\
\frac{\tau_2}{l_2} &= \ddot{\alpha} l_1 m_2 + \ddot{\beta} l_2 m_2 \\
\text{COM}_x &= -\frac{\alpha l_1 m_1 + \alpha l_1 m_2 + \beta l_2 m_2}{m_0 + m_1 + m_2}
\end{aligned} \tag{7}$$

Rearranging, we see that

$$\begin{aligned}
\ddot{\alpha} &= \frac{\tau_2 (-l_1 - l_2)}{l_1^2 l_2 m_1} \\
\ddot{\beta} &= \frac{l_1 \ddot{\alpha} (-l_1 m_1 - l_1 m_2 - l_2 m_2)}{l_2 m_2 (l_1 + l_2)}
\end{aligned} \tag{8}$$

From (7) and (8), we can see that $\frac{d^2 \text{COM}_x}{dt^2}$ is proportional to $\ddot{\alpha}$ and $\ddot{\beta}$, and therefore proportional to τ_2 .

For the LQR controller, we use state penalties on the order of 10^8 times the input penalty — this facilitates aggressive hip action. The LQR controller produces values for hip torque τ_2 which are directly applied at the hip. To obtain a desired foot angle, we use the following equation:

$$\begin{aligned}
\gamma &= -\sin^{-1}(\text{COM}_x) + \begin{cases} -C_2, & \text{if } \text{COM}_x > 0 \\ C_2, & \text{if } \text{COM}_x \leq 0 \end{cases} \\
\theta_{\text{target}} &= \text{clip}(\gamma, [-\frac{\pi}{6}, \frac{\pi}{6}])
\end{aligned} \tag{9}$$

Here, C_2 is a constant that is tuned to a small positive value so that the foot angle stays relatively smooth when switching from Case 2 to Case 3. This constant is necessary because when the controller switches from Case 2 to Case 3, the hip movement suddenly becomes much less aggressive; this sudden acceleration can cause discontinuities in the target foot angle. Additionally, we clip the angle to preserve reasonable ranges of motion. If the foot angle is not clipped, it is possible to have the person's foot to be almost vertical, which is unrealistic. Finally, we apply a PID controller to track this angle subject to foot dynamics.

C. Case 3

The Case 3 controller is applied when the COM is close to equilibrium but the torso angle is far from equilibrium. As with the other cases, we use an LQR controller in the upper layer: in this case, we use two controllers, one for the hip

and one for the ankle. For the LQR controllers, we use state penalties on the order of 10-100 times the input penalty.

For the hip controller, we build a linearized model of state dynamics; the states are β and $\dot{\beta}$ and the input is τ_2 . We then apply LQR to the linearized model to obtain a controller. The equations of motion simplify to

$$\ddot{\beta} = C_3 \tau_2 \tag{10}$$

where C_3 is some constant. This system has similar equations of motions as Case 2, so C_3 can be derived from (7) and (8) in a similar way as shown above. Here, even though the movement is slow, we ignore the effect of θ .

For the ankle controller, we build a linearized model. The states are COM_x and its derivative, and the control is x_{contact} . The equations of motion are similar to Case 1, except we now have a double pendulum instead of a single pendulum:

$$\frac{d^2 \text{COM}_x}{dt^2} = g(\text{COM}_x + x_{\text{contact}})/L + C_4 \ddot{\beta} \tag{11}$$

where C_4 can be derived from (7) and (8). Here, $\ddot{\beta}$ is treated as an exogenous signal, which is received from the hip LQR controller. Thus, the ankle planner takes into account the hip's movements, while the hip planner does not take into account the ankle's movements. It turns out that this one-way coordination is sufficient for stability, as shown in simulations.

The hip LQR controller produces values for hip torque τ_2 which are directly applied to the hip. The ankle LQR controller's output is converted to a desired target angle θ using 4; a PID controller is applied to track this desired target angle subject to foot dynamics.

IV. SIMULATIONS

Simulation results show that our controller is able to maintain stability and restore equilibrium posture if the the initial value of COM_x is within the range of $[-5, 9.6]$ cm to the equilibrium, for a log radius of 10cm. Moreover, throughout all simulations, hip and ankle angles were within the biological ranges of motion. We simulated the nonlinear equations of motion (1) using the 4th-order Runge-Kutta method with a time-step of 20 ms.¹

Figure 4 shows the COM trajectories for a variety of initial conditions, in the absence of noise. All trajectories converge to the equilibrium posture; additionally, all trajectories go through Case 2, then Case 3, and end in Case 1. The controller is also tolerant to Gaussian sensory noise, as demonstrated in Figure 5, which shows the COM trajectories for a variety of initial conditions. A video of the simulation corresponding to the blue line in this figure can be found at <https://www.youtube.com/watch?v=g7qfnd7hzqA>.

Figure 6 shows ankle angle, hip angle, and COM trajectories over time for a single simulation. As expected, the angular values are restored to equilibrium. We notice that while the ankle angle exhibits rapid fluctuations between

¹We note that this method is numerically sensitive and requires very small time-steps (on the order of milliseconds) when $\text{COM}_x < 0$.

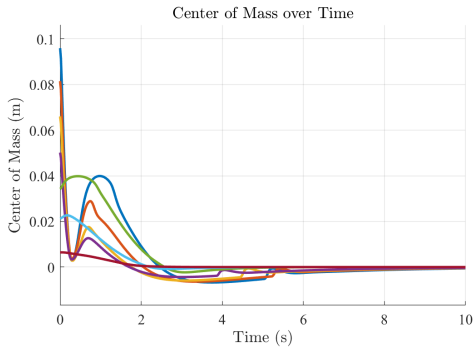


Fig. 4. COM trajectories over time for 7 different initial conditions. In all cases, the controller stabilizes the system and returns the human to the equilibrium posture.

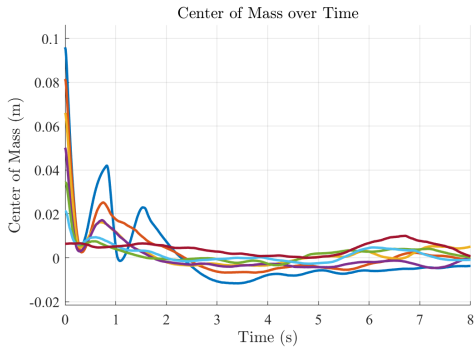


Fig. 5. COM trajectories over time for 7 different initial conditions, with zero-mean Gaussian sensory noise. The noise on COM_x , its derivative, angle, and angular velocity have standard deviation of 0.01m, 0.005m/s, 0.01 rad, and 0.005 rad/s respectively. The blue line with initial $COM_x = 96cm$ shows an extreme case when the controller enters case 2 a second time after entering case 3 due to sensory error. We can see two peaks in the blue line. The second peak is much lower than the first peak. Our controller is still able to make COM_x converge properly in this condition. This shows that our three case control system has the potential of handling cases with a wider range of COM_x .

$t=0$ and $t=1$, the hip motion is relatively smooth throughout. Interestingly, this is reminiscent of human balancing, which involves rapid ankle fluctuations and slower hip movements². The controller is in Case 2 for less than a second, demonstrating that the Case 2 controller restores balance (e.g. lowers the COM deviation) very rapidly. The controller spends about 5 seconds in Case 3, during which the hip angle is slowly brought toward the equilibrium value. After 5 seconds, the controller returns to and stays in Case 1.

Figure 7 shows the real foot angle and target foot angle over a single simulation (reminder: foot angle is θ ; not to be confused with ankle angle, which is $0.5\pi + \alpha - \theta$). The target angle is generated by the upper layer controller (subject to linearity assumptions), and the lower layer controller tracks this value. In general, we see that tracking is satisfactory, particularly after the initial quick changes in target angle — more importantly, as shown in Fig. 6, the conjunction of the upper and lower layer controllers results in successful

²as a “hands-on activity”, we invite the reader to try balancing on a non-flat object and observe their own hip and ankle movements

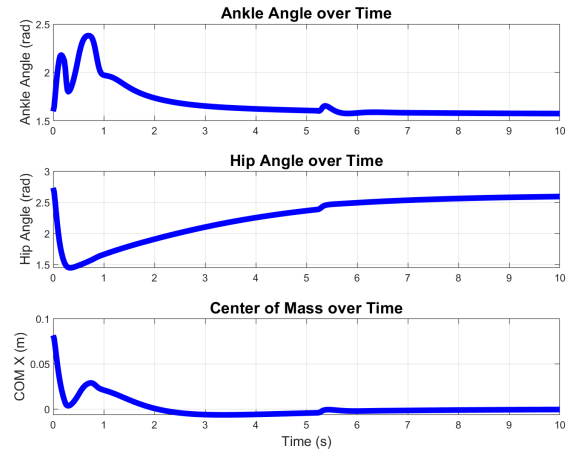


Fig. 6. Ankle angle, hip angle, and COM trajectories over time for a single simulation. Here, equilibrium values for hip and ankle are 2.6 and 1.57 respectively. The controller is initially in Case 2; this causes a sharp decrease of hip angle from $t=0$ to around $t=0.3$ in order to restore the COM value to near-equilibrium. After this point, Case 3 is used, and slowly restores the hip angle to equilibrium while maintaining near-equilibrium COM. The controller switches to Case 1 around $t=5.2$

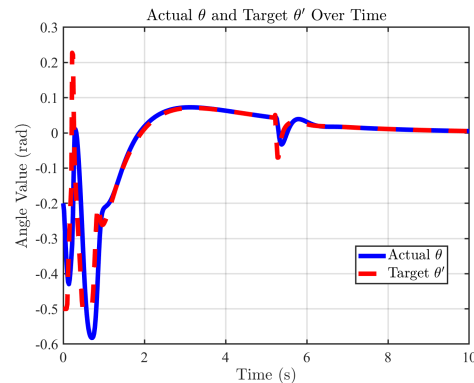


Fig. 7. The actual foot angle θ and the target foot angle θ' for one simulation run. After some transient behavior (during which the target angle changes rapidly), the PID controller tracks the target angle quite well. Note that the equilibrium foot angle is $\theta = 0$.

balancing.

V. TOWARDS BIOMECHANICAL REALISM

We have showed that our torque-based controller can successfully balance the human on a log. We are now interested in incorporating more biomechanical features into the plant and controller, so that we can gain more insights into human motor control. In particular, we will focus on achieving control in the small-COM small-angle case (i.e. Case 1) using muscle control as opposed to torque control, and defer muscle control of the other two cases to future work. We also briefly explore how imperfect sensing (as is common in biology) may be incorporated into our controller.

Torque actuators for joints are common in robotics, but nonexistent in animals. For humans, the central nervous system sends signals to muscles, which contract and/or relax

to produce forces that result in changes of joint angle. A simplified model of the muscles involved in hip and ankle movement is shown in Figure 8. Each muscle receives neural activation from the central nervous systems which results in muscle contraction; we assume that the resulting muscle force is proportional to the neural activation level on the muscle (i.e. muscle activation) [9]. Equations of motion relating muscle activation levels to resulting torques are derived using techniques from [10]. For simplicity, we ignore the effects of length changes and temperature/velocity on muscle behavior, and focus primarily on muscles as force actuators.

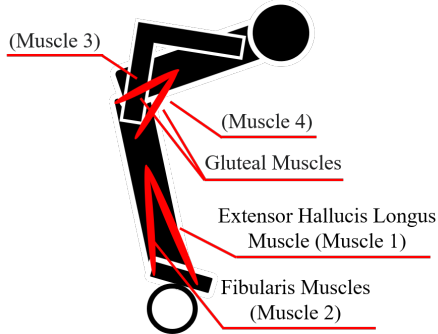


Fig. 8. Schematic of muscle-based model for the log-balancing task. Instead of applying torques to the ankle and hip joints, we manipulate the joints using simplified muscle groups; the gluteal muscles actuate the hip, and the remaining muscles actuate the ankle. The simulation with muscles are conducted by calculating the torques provided by corresponding muscle pairs and updated with the torque model.

We use small-angle approximations to linearize the equations of motion about the equilibrium posture. The resulting linear system has the foot, leg, and torso angle and angular velocities as the states (i.e. $\theta, \alpha, \beta, \dot{\theta}, \dot{\alpha}, \dot{\beta}$). Note that in the small-COM case, we actually do not need to account for COM explicitly in our equations — though an interesting avenue of future exploration is how COM may be sensed or estimated from state variables, and how this can affect control in the large-COM case. The control inputs to the linear system are muscle activation levels. Without considering COM, there is less need for the two-layer controller, and we directly design a single LQR controller using this linearized system.

The outputs of the LQR controller cannot be directly applied to the system. This is because muscle forces are generated primarily through contraction, and cannot be negative — thus, muscle activation levels also cannot be negative. However, the LQR controller outputs negative control values. We devise a post-compensation strategy to avoid negative muscle activation levels. Our strategy is inspired by agonist-antagonist muscle pairings in animals. In general, for a given joint, there are two (or more) muscles that can move the joint — often, one muscle (the “agonist”) contracts while the other (the “antagonist”) relaxes [11]. In our model, muscles 3 and 4 form an agonist-antagonist pair, and muscles 1 and 2 form an agonist-antagonist pair. Thus, if the LQR controller outputs a negative muscle activation level for one of the muscles, we

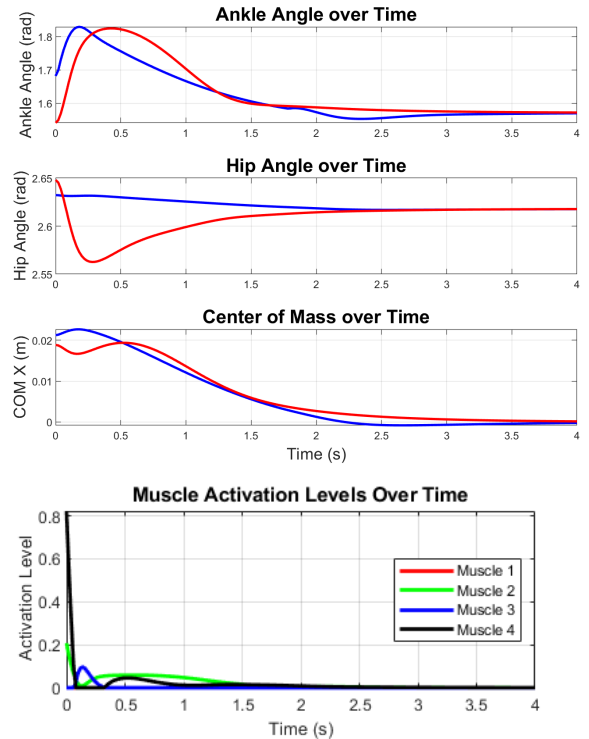


Fig. 9. Top 3 plots: ankle angle, hip angle, COM over time for a single simulation with small initial condition using the muscle controller (red) and torque controller (blue). The torque controller stays in Case 1 for the whole simulation. The ankle and COM trajectories are similar between the two controllers; the hip angles are slightly different due to the different hip control strategies. Both controllers restore the person to equilibrium posture; here, equilibrium values for hip and ankle are 2.6 and 1.57 respectively. Bottom plot: muscle activation trajectories over time. Muscles 2-4 are used to bring the human back to the equilibrium posture in under 3 seconds; muscle 1 is not used in this simulation. The maximum force of muscles are all set to be 800 N, and the activation level cannot exceed 1.

shift this into an equivalent positive muscle activation level on the antagonist muscle. As an example, for the system

$$\dot{x}(t) = Ax(t) + \begin{bmatrix} b_1 & b_2 \\ b_3 & b_4 \end{bmatrix} \begin{bmatrix} u_1(t) \\ u_2(t) \end{bmatrix}, \quad (12)$$

where $b_1 b_2 < 0$ and $b_3 b_4 < 0$ due to the symmetry between agonist-antagonist pairs. Let $u^{lqr} = Kx$ be the control input from the LQR controller at some point in time, and assume that the state penalty matrix Q is diagonal. If $u^{lqr} > 0$, then we can simply set $u = u^{lqr}$. However, if $u_1^{lqr} < 0$, then we compensate by setting $u_1 = 0$ and setting

$$u_2 = u_2^{lqr} - \frac{Q_{1,1}}{Q_{1,1} + Q_{2,2}} \frac{b_1}{b_2} u_1^{lqr} - \frac{Q_{2,2}}{Q_{1,1} + Q_{2,2}} \frac{b_3}{b_4} u_1^{lqr} \quad (13)$$

A similar compensation can be done if $u_2^{lqr} < 0$. In the (unlikely) case where both u_1^{lqr} and u_2^{lqr} are negative, we can simultaneously compensate via:

$$u = \begin{bmatrix} -\frac{Q_{1,1}}{Q_{1,1} + Q_{2,2}} \frac{b_2}{b_1} u_2^{lqr} - \frac{Q_{2,2}}{Q_{1,1} + Q_{2,2}} \frac{b_4}{b_3} u_2^{lqr} \\ -\frac{Q_{1,1}}{Q_{1,1} + Q_{2,2}} \frac{b_1}{b_2} u_1^{lqr} - \frac{Q_{2,2}}{Q_{1,1} + Q_{2,2}} \frac{b_3}{b_4} u_1^{lqr} \end{bmatrix}. \quad (14)$$

These compensation strategies ensure that the resulting behavior remains optimal while respecting the physiological

constraint that muscle activation levels cannot be negative. One reason we opt for a single-layer LQR controller in this case (as opposed to the two-layer controller in the torque-based control) is that the single-layer LQR allows us to devise a simple compensation strategy. Developing compensation strategies for layered controllers will be explored in future works.

Remark: Joint torques are uniquely determined by muscle forces, but muscle forces are not uniquely determined by joint torques — for a given joint torque, there are many possible muscle force combinations that would elicit this torque. Thus, one way of adapting the full three-case torque controller to muscle control is to find the torques, then convert them to muscle forces. However, this can result in some suboptimality in muscle forces (e.g. the desired torques may require unnecessarily large values of muscle force). Additionally, it is unclear whether such a torque-to-muscle conversion is biologically realistic (i.e. whether the nervous system actually does any computations in torque coordinates). Thus, we are interested in exploring how we can directly design muscle control and use principles from layered control (as in Case 2 and Case 3) to do so.

We are additionally interested in incorporating estimation into our model. In general, humans deal with imperfect sensing, and often use sensory information to provide estimates on unsensed quantities [12]. We incorporate this into our model by removing sensory information on one of the angle/angular-velocity states, and using the remaining states to estimate the missing state via a Kalman filter. We show one such simulation in Figure 9 (red line); generally, the controller behaves well no matter which sensor is removed. Additionally, we see that the COM and ankle angles produced by the muscle-based controller quantitatively resemble that of the torque controller shown in the same figure (blue line). Both simulations start around 0.02cm of COM deviation from equilibrium, and return to 0cm within 3 seconds. The trajectory of COM is qualitatively similar, with a small increase in the beginning and a gradual smooth decrease. The primary difference is in the hip angle; the torque-based model exhibits little hip movement while the muscle model exhibits some movement. This discrepancy arises from the fact that the torque-based controller explicitly forces the hip to be stiff, whereas no such forcing occurs in the muscle-based model.

In this section, we have provided a brief exploration of how the log-balancing controller described in this paper can be extended to feature more biomechanical elements. Extending the full 3-case controller with biologically realistic muscles and sensors will be a topic of future work.

REFERENCES

- [1] Y. Ivanenko and V. S. Gurfinkel, "Human postural control," *Front Neurosci*, vol. 12, p. 171, Mar. 2018.
- [2] Y. Kanamiya, S. Ota, and D. Sato, "Ankle and hip balance control strategies with transitions," in *2010 IEEE International Conference on Robotics and Automation*. IEEE, 2010, pp. 3446–3451.
- [3] L. Muhsen and N. Maan, "Lie group analysis of retarded delay differential equations in human postural balance model," *International Journal of Mathematical Analysis*, vol. 9, pp. 2303–2318, 10 2015.

- [4] J. E. Barton, A. Roy, J. D. Sorkin, M. W. Rogers, and R. Macko, "An engineering model of human balance control-part i: Biomechanical model," *J. Biomech. Eng.*, vol. 138, no. 1, p. 014502, Jan. 2016.
- [5] A. Kuo, "An optimal control model for analyzing human postural balance," *IEEE Transactions on Biomedical Engineering*, vol. 42, no. 1, pp. 87–101, 1995.
- [6] K. Iqbal, "Mechanisms and models of postural stability and control," in *2011 Annual International Conference of the IEEE Engineering in Medicine and Biology Society*, 2011, pp. 7837–7840.
- [7] Y. Nakahira, Q. Liu, T. J. Sejnowski, and J. C. Doyle, "Diversity-enabled sweet spots in layered architectures and speed–accuracy trade-offs in sensorimotor control," *Proceedings of the National Academy of Sciences*, vol. 118, no. 22, p. e1916367118, 2021.
- [8] L. Karashchuk, J. S. L. Li, G. M. Chou, S. Walling-Bell, S. L. Brunton, J. C. Tuthill, and B. W. Brunton, "Sensorimotor delays constrain robust locomotion in a 3d kinematic model of fly walking," *eLife*, Aug. 2024. [Online]. Available: <http://dx.doi.org/10.7554/eLife.99005.1>
- [9] P. Greene, A. J. Bastian, M. H. Schieber, and S. V. Sarma, "Optimal reaching subject to computational and physical constraints reveals structure of the sensorimotor control system," *Proceedings of the National Academy of Sciences*, vol. 121, no. 14, p. e2319313121, 2024.
- [10] W. Li and E. Todorov, "Iterative linear quadratic regulator design for nonlinear biological movement systems," in *First International Conference on Informatics in Control, Automation and Robotics*, vol. 2. SciTePress, 2004, pp. 222–229.
- [11] D. Kim and J.-M. Hwang, "The center of pressure and ankle muscle co-contraction in response to anterior-posterior perturbations," *PLoS One*, vol. 13, no. 11, p. e0207667, Nov. 2018.
- [12] H. Tanaka, T. Ishikawa, J. Lee, and S. Kakei, "The cerebro-cerebellum as a locus of forward model: A review," *Front. Syst. Neurosci.*, vol. 14, Apr. 2020.